

Spontaneous increase of magnetic flux and chiral-current reversal in bosonic ladders: Swimming against the tide

S. Greschner,¹ M. Piraud,² F. Heidrich-Meisner,² I. P. McCulloch,³ U. Schollwöck,² and T. Vekua¹

¹*Institut für Theoretische Physik, Leibniz Universität Hannover, 30167 Hannover, Germany*

²*Department of Physics and Arnold Sommerfeld Center for Theoretical Physics,
Ludwig-Maximilians-Universität München, 80333 München, Germany*

³*ARC Centre for Engineered Quantum Systems, School of Mathematics and Physics,
The University of Queensland, St Lucia, QLD 4072, Australia*

(Dated: March 19, 2019)

The interplay between spontaneous symmetry breaking in many-body systems, the wave-like nature of quantum particles and lattice effects produces an extraordinary behavior of the chiral current of bosonic particles in the presence of a uniform magnetic flux defined on a two-leg ladder. While non-interacting particles, stirred by the magnetic field and for values of the flux between a quarter and half-a-flux quantum, circulate along the system's boundary in the counterclockwise direction, for arbitrarily weak interactions between particles and at sufficiently low temperature, the circulation direction can be spontaneously reversed. For the Bose-Hubbard model on the two-leg ladder, the spontaneously symmetry broken states are vortex lattices. Our predictions could readily be accessed in quantum gas experiments with existing setups or in arrays of Josephson junctions.

The Lorentz force, $F_L = q\mathbf{v} \times \mathbf{B}$ induced by the magnetic field \mathbf{B} causes the path of a particle with electric charge q to bend perpendicular to the direction of the particle's velocity \mathbf{v} . The orientation of the magnetic field with respect to the particle's velocity and the sign of q determine whether the bending of the path happens in a clockwise or a counterclockwise fashion, giving a definite handedness or chirality to the particle current. If the motion of particles is restricted to a straight line, a magnetic field has no effect, since there is no way for a bending of the path. Yet, as soon as transverse motion is allowed, as is the case for the ladder-like geometry depicted in Fig. 1, a magnetic field applied perpendicular to the plane of the ladder will induce a chiral current. A *quantum particle*, due to its wave-like nature [1], has a phase. While moving around a closed path in a magnetic field, a charged particle picks up an increment to its phase proportional to the magnetic flux piercing the area enclosed by the path. If the particle hops around a plaquette (cf. Fig. 1), the accumulated phase is proportional to the magnetic flux $\Phi = Ba^2$ piercing the unit cell \square , a being the lattice constant. Since the phase of the wavefunction is defined modulo 2π , the action of a magnetic field on quantum particles in a lattice is periodic: If we define a dimensionless flux $\phi = 2\pi\Phi/\Phi_0$ with the magnetic flux quantum $\Phi_0 = h/q$, where h is Planck's constant, any physical quantity \mathcal{A} obeys $\mathcal{A}(\phi) = \mathcal{A}(\phi + 2\pi)$.

For a macroscopic number of indistinguishable particles at low temperatures quantum statistics starts to imprint itself onto many-body behavior and as a result, bosonic particles undergo Bose-Einstein condensation [2–5]. Interactions and quantum correlations bring in fascinating effects such as superfluidity [6–9]. A famous manifestation of superfluidity emerges under rotations (or, for charged superfluids, under the action of a magnetic field), where beyond a critical rotation frequency, quan-

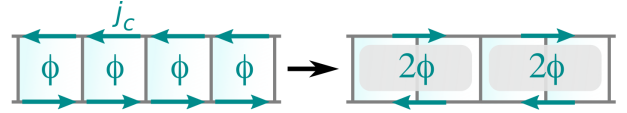


FIG. 1. *Sketch of the effective doubling of the magnetic flux.* A spontaneous breaking of invariance under discrete lattice translations results in a doubling of the unit cell (here, the cell denoted by \square is doubled, i.e., $\square \rightarrow \square\square$) and hence the flux piercing the new unit cell doubles as well: $\phi \rightarrow 2\phi$. Under the conditions described in the text, the chiral current j_c , the sum of local currents indicated by the arrows circulating along the boundary \mathcal{B} of the ladder, reverses its direction.

tized vortices appear [10–15]. These vortices can arrange themselves in regular vortex lattices [13, 14, 16–18].

In this work, we discuss the intriguing effect of a *reversal* of the circulation direction of the chiral current of interacting bosons in the two-leg ladder system of Fig. 2a, due to the spontaneous formation of a large unit cell (see Fig. 1) *without* changing the external magnetic field. The key ingredients to realize this effect are, first, the wave-like nature of quantum particles defined on a lattice, and second, many-body effects.

Chiral-current reversal. The basic idea is sketched in Fig. 1. Consider particles hopping on a lattice with flux ϕ per unit cell \square . For a single plaquette, the magnetic fields corresponding to values of the flux $0 < \phi < \pi$ produce a ground-state net current with a counterclockwise chirality. When one assembles these plaquettes into a minimal extensive lattice such as the two-leg ladder, naively, one would expect that the local currents $j_{l,\mathcal{B}}$ on individual links along the boundary \mathcal{B} of the ladder add up to produce a net chiral current j_c circulating also in counterclockwise direction for $0 < \phi < \pi$. Indeed, this is the case for non-interacting particles [19]. In general, since the chiral current is a ground-state property, the

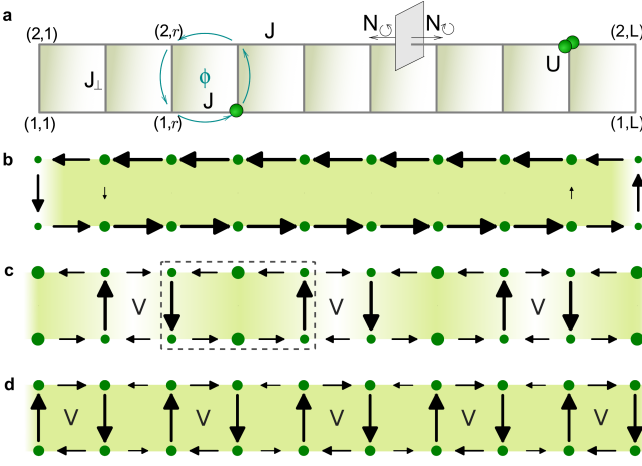


FIG. 2. *Sketch of the model and typical current patterns.* **a**, A two-leg ladder with L rungs and a uniform flux ϕ per plaquette. **b-d**, Local currents and onsite densities in the Meissner phase (**b**), the vortex-lattice superfluid phase at vortex density $\rho_v = 1/3$ (**c**) and the vortex-lattice superfluid phase at $\rho_v = 1/2$ (**d**) [$U = 2J$, $J_\perp = 1.6J$, $\rho = 0.8$ and $\phi = 0.6\pi$ (**b**), 0.8π (**c**) and 0.9π (**d**)]. The length of the arrows encodes the strength of local currents and the size of the circles is proportional to the onsite density. Density modulations are also visualized by the shading, with lighter green corresponding to lower density. In **c**, a Meissner-like region is indicated by the dashed line. The chiral current is reversed in **d**, but not in **b** and **c**. In **a**, $L = 10$, while **b** and **c** show the behavior in the bulk of a system with $L = 120$.

relevant unit cell does not need to be the same as the unit cell of the underlying lattice.

If the unit cell is spontaneously enlarged such that $\square \rightarrow \square\square$, then this will result in a doubling of the effective flux $\phi_{\text{eff}} = 2\phi$, piercing the enlarged unit cell of the ground state. The chiral current j_c is an odd function of the magnetic field and periodic, thus $j_c(\phi) = j_c(\phi - 2\pi) = -j_c(2\pi - \phi)$. As a consequence, for values of the flux $\pi/2 < \phi < \pi$ defined with respect to the original cell, the effective flux is in the domain $\phi_{\text{eff}} \in (-\pi, 0)$ modulo 2π , which one would also obtain if the orientation of the magnetic field was inverted. The doubling of the unit cell is a consequence of the spontaneous breaking of discrete lattice translation symmetry.

Model. We study the single-band Bose-Hubbard model:

$$H = -J \sum_{\substack{r=1 \\ \ell=1,2}}^{L-1} (a_{\ell,r+1}^\dagger a_{\ell,r} + \text{H.c.}) + \frac{U}{2} \sum_{\substack{r=1 \\ \ell=1,2}}^L n_{\ell,r} (n_{\ell,r} - 1) - J_\perp \sum_{r=1}^L (e^{-ir\phi} a_{1,r}^\dagger a_{2,r} + \text{H.c.}). \quad (1)$$

$a_{\ell,r}^\dagger$ creates a boson on the lower ($\ell = 1$) or the upper site ($\ell = 2$) of the r -th rung, $n_{\ell,r} = a_{\ell,r}^\dagger a_{\ell,r}$, and L is the number of rungs. The hopping matrix elements between the

nearest-neighbor sites along the ladder's legs and rungs are denoted by J and J_\perp , respectively, and U is the repulsive onsite interaction. The filling is $\rho = N/(2L)$, where N is the number of bosons. We carried out density matrix renormalization group (DMRG) simulations [20, 21] for $\rho < 2$ and $U \gtrsim J$. For the complementary regime of large densities $\rho \gg 1$ and weak interactions $U \ll J$ we use a mapping to a frustrated XY model and apply a transfer-matrix approach [22, 23]. Details on both techniques are provided in the Methods section.

Physical realizations are, for instance, either arrays of Josephson junctions of superconducting islands in a magnetic field [24–26], where the bosonic particles are Cooper pairs of electrons with $q = 2e$, or neutral ultracold bosons in optical lattices [27, 28] in the presence of artificial gauge fields, subject to s-wave interactions [29–31]. In the latter case, the effect of a magnetic field is mimicked by laser-assisted hopping [29–31] between neighboring sites, imprinting the spatially varying phase of the laser onto the atomic wave function.

Meissner and vortex phases. For the two-leg ladder, the existence of Meissner-like and vortex phases has been firmly established both in the weakly- and strongly-interacting regime [19, 32–36]. In Fig. 2b, obtained from a numerical DMRG simulation, we depict the typical behavior of local currents and particle densities in the low-field Meissner phase. The currents are non-zero along the boundary of the two-leg ladder \mathcal{B} , which consists of the edge rungs and the legs of the ladder, and vanish quickly on the inner rungs away from the first and last rung, producing a net chiral current that is the sum of local currents defined on the boundary links $j_c = \sum_{l \in \mathcal{B}} \dot{j}_{l,\mathcal{B}}/N$ (see supplemental Sec. S1 for definitions and properties of j_c). Here, $\dot{j}_{l,\mathcal{B}} \sim \dot{N}_\square^l - \dot{N}_\square^l$ is the expectation value of the local current operator on a link on the ladder's boundary and the dot denotes the time derivative. Thus, $\dot{j}_{l,\mathcal{B}}$ measures the difference between counterclockwise (\dot{N}_\square^l) and clockwise rotating (\dot{N}_\square^l) particles passing, in a unit of time, through a surface (indicated by the shaded area in Fig. 2a) that cuts a link l of \mathcal{B} . It is the coherence of the relative phase of bosons on the two legs that induces the Meissner phase in bosonic ladders [22, 37] and hence a chiral current can also emerge in the Mott-insulator regime for fillings with an integer number of particles per rung [32, 35]. The behavior of currents in the Meissner phase of the ladder is reminiscent of the behavior of currents in superconductors in the low-field Meissner [38] regime, where currents in the bulk vanish and only a screening edge current is present.

Upon increasing the magnetic field beyond a critical value, resembling the lower critical magnetic field H_{c1} in type-II superconductors [16], the system enters into a vortex phase where local currents on the inner rungs develop, resulting in a current configuration that is reminiscent of a Meissner phase disordered with vortices [22, 35, 37]. These vortices interact repulsively with

each other [22], yet for generic vortex densities ρ_v , they are distributed in the system without any periodicity, similar to molecules in liquids. At certain commensurate vortex densities, however, vortex lattices (VL) can form in the ground state [22, 37]. In these VLs, vortices exhibit strictly periodic arrangements, like molecules in a crystalline solid. Examples of such VL states, obtained from DMRG simulations of equation (1), are depicted in Figs. 2c and d. In the VL superfluid at vortex density $\rho_v = 1/3$ (denoted by $\text{VL}_{1/3}\text{-SF}$, see supplemental Sec. S3 for more details) shown in Fig. 2c, the currents on two neighboring plaquettes form a complex (surrounded by a dashed line in Fig. 2c) that is a mini copy of the Meissner phase (with 'screening' currents circulating around the complex' boundary and vanishing currents on its inner rung) such that on every third plaquette, a vortex resides, around which the current circulates in the direction opposite to the behavior in the Meissner phase. In the example shown in Fig. 2c, the chiral current goes in the counterclockwise direction. In the vortex lattice at $\rho_v = 1/2$ ($\text{VL}_{1/2}\text{-SF}$), obtained for a flux value close to half-a-flux quantum, a vortex sits on every other plaquette, as shown in Fig. 2d, and the direction of the chiral current is reversed.

Experimentally, the chiral current was measured in a system of bosonic atoms in an optical lattice that realizes the two-leg ladder of Fig. 2a as a function of J_\perp , for flux values of $\phi \simeq \pm\pi/2$, a weak interaction and in the high-density regime [29]. The behavior of the chiral current has also been the central object of recent experiments with bosonic [39] (realizing fluxes $\phi \simeq \pm 2\pi/3$) as well as fermionic [40] (realizing fluxes $\phi \simeq \pm 0.37\pi$) ultracold quantum gases, effectively realizing two- and three-leg ladders. In the latter two studies [39, 40], the sites along the rung direction correspond to the different hyperfine states, forming a synthetic lattice dimension [41].

Interaction-driven chiral-current reversal. For intermediate values of $J_\perp/J \sim \mathcal{O}(1)$, not too low particle densities and flux values close to π , we generically observe a reversal of the chiral current tuned by the interaction strength U/J : j_c flows in a counterclockwise direction along the ladder's legs for $U = 0$ and $U \rightarrow \infty$, yet for a certain range of interaction strengths at low temperatures the circulation direction of the current is reversed, as if the majority of particles *swam against the tide*.

The interaction driven chiral-current reversal is evident from the DMRG results presented in Fig. 3. There, we plot the chiral current as a function of interaction strength for three different values of the densities corresponding to odd integer, fractional, and even integer fillings per ladder rung (i.e., $\rho = 0.5$, 0.8 , and $\rho = 1$, respectively). We clearly numerically resolve a current reversal in all three cases at sufficiently large values of $U/J \sim 1$, which is tied to the presence of the vortex-lattice at $\rho_v = 1/2$ which can be realized both in the superfluid ($\text{VL}_{1/2}\text{-SF}$) and the Mott-insulating regime

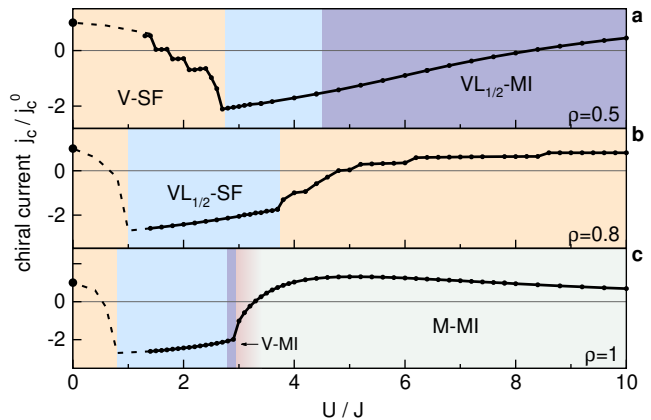


FIG. 3. *Chiral current versus interaction strength.* **a-c**, We consider the behavior in the proximity of the vortex-lattice phases at $1/2$ vortex density that can be either superfluids ($\text{VL}_{1/2}\text{-SF}$) or Mott insulators ($\text{VL}_{1/2}\text{-MI}$), for $\phi = 0.9\pi$, $J_\perp = 1.6J$ and different fillings: $\rho = 0.5$ (**a**), $\rho = 0.8$ (**b**), and $\rho = 1$ (**c**) (DMRG data for $L = 160$). For $\rho = 1$ (**c**) the following Mott-insulating phases are realized with increasing $U/J \leq 10$: a $\text{VL}_{1/2}\text{-MI}$, a vortex Mott-insulator (V-MI), and finally, a Meissner Mott-insulator (M-MI). The numerical data for the vortex superfluids (V-SF, orange) at small U/J are reliable for interactions larger than $U \simeq 1.5J$; the dashed lines are guides to the eye. The exact value for $U = 0$ is $j_c^0 \simeq 0.08J > 0$, independently of ρ . The small steps seen in the V-SF phase are finite-size effects (see Fig. 4 and Sec. S2).

($\text{VL}_{1/2}\text{-MI}$). The $\text{VL}_{1/2}\text{-SF}$ phase is neighbored by a vortex superfluid for small values of U/J . In the normalization adopted in Fig. 3, the value of the chiral current is independent of ρ and positive at $U = 0$, implying that in all cases, the chiral current undergoes a sign change in the vortex-liquid phases as the transitions to either one of the two vortex-lattice states are approached. Generally, upon entering into the vortex-liquid phases from the vortex-lattice phases, the absolute value $|j_c|$ of the current decreases continuously for $L \rightarrow \infty$ (while for finite L , small steps are seen), showing a cusp-like behavior at the phase boundary (see also supplemental Fig. 8). Other transitions that are crossed in Fig. 3 do not leave a fingerprint in the interaction dependence of j_c for $L \rightarrow \infty$.

Further increasing U/J takes the system from the $\text{VL}_{1/2}\text{-SF}$ into a $\text{VL}_{1/2}\text{-MI}$ for $\rho = 0.5$ (see Fig. 3a) or back into the V-SF for $\rho = 0.8$ (see Fig. 3b). The Mott-insulating region at $\rho = 1$ (shown in Fig. 3c) is much richer since the following phases are realized with increasing U/J : a narrow $\text{VL}_{1/2}\text{-MI}$, a vortex Mott-insulator (V-MI), and finally, a Meissner Mott-insulator state (M-MI). For a discussion of the phases at $\rho = 1$ and $\phi = \pi$ see [42, 43].

For all values of ρ considered in Fig. 3, the sign of the chiral current becomes positive again on the large U/J side. The chiral-current reversal is thus robust against

the presence or absence of a mass gap and a variation of density. Moreover, the absolute value of the reversed chiral current can exceed the $U = 0$ value by a factor of three.

The spontaneous symmetry-breaking leading to the M -times enlarged unit cell with $\phi_{\text{eff}} = M\phi \in (-\pi, 0)$ modulo 2π ($M = 2$ in Fig. 3) is a vital ingredient for obtaining the current reversal. We argue that yet another requirement is that the dominant contribution to the current comes from particles with a large wavelength experiencing the effective flux when propagating along the ladder legs. This is exemplified by the behavior of the chiral current in the fully gapped, Mott-insulating vortex lattice (the VL $_{1/2}$ -MI, see Fig. 3a): Inside this state with a doubled unit cell, the chiral current, as a function of U/J , passes through zero and returns back to the original direction of rotation, the latter the behavior of free particles. The reason is that the localization length of bosons in the Mott-insulating phase becomes shorter with increasing U/J , restricting the typical wave-lengths of particles and as a consequence, less particles see the enlarged unit cell with doubled flux. On these grounds, we expect that in a given phase with a spontaneously enlarged unit cell, the absolute value of the reversed chiral current attains its maximum for the smallest U/J in that phase, consistent with the data presented in Fig. 3. We emphasize that the optimal condition for observing the current reversal in two-leg ladders is a doubling of the unit cell.

In the supplemental material (Sec. S3), we present the phase diagrams in the parameter plane (ϕ, J_{\perp}) (shown in Fig. 6a) for $U/J = 2$ and a non-integer filling and in the plane $(\rho, U/J)$ (shown in Fig. 6b) for $\phi = 0.9\pi$. This serves the purpose of identifying the regions in parameter space spanned by ϕ , U , ρ and J_{\perp} , in which the vortex-lattice phases exist, whose presence is required for the chiral-current reversal effect. We also present the behavior of local currents and particle densities in different phases (Sec. S4, Figs. 7 and 9).

Finite temperatures. Since the current reversal is connected with spontaneous symmetry breaking in the ground state, a relevant question pertains to the effect of temperature. First, we stress that the current reversal, at $T = 0$, is not sharply tied to the phase boundaries of the vortex-lattice states, but survives a finite density of defects as one can see in Fig. 3. This gives confidence that temperature will not wash out the reversal immediately, as opposed to the long-range crystalline order of VL states. To obtain a quantitative understanding of the effect of a finite temperature, we consider the limit of large particle densities $\rho \gg 1$ and weak interactions $U/J \ll 1$. Using the transfer-matrix approach [23], we obtain the results shown in Fig. 4, where the chiral current (Fig. 4a) and vortex density (Fig. 4b) versus flux are presented for different temperatures. For $\rho \gg 1$, upon reducing temperature, vortex lattices ap-

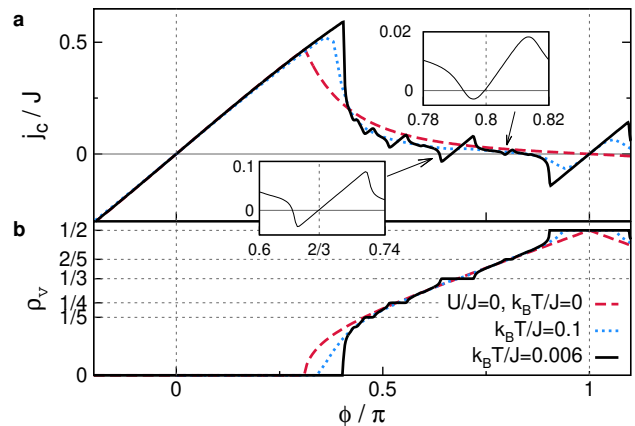


FIG. 4. *Weak-coupling regime* $\rho \gg 1$, $U/J \rightarrow 0$. **a, b**, Chiral current (in units of J) (**a**) and vortex density (**b**) as a function of flux for $\rho \gg 1$, $U/J \rightarrow 0$ and $J_{\perp} = J/2$. The chiral current shows a reversal at low temperatures in vortex-lattice states with $\rho_v = 1/3, 2/5, 1/2$. The temperature is $k_B T = 0.006J$ (continuous lines) and $k_B T = 0.1J$ (dotted lines); the dashed lines are for $U = 0$ at $T = 0$. The current stays reversed for $\phi \simeq 0.9\pi$ up to $k_B T \simeq 0.2J$, whereas for other values of ϕ , the reversal disappears much faster with T .

pear at $\rho_v = 1/2, 1/3, 2/5, 1/4, 1/5, \dots$. These have an $M = 2, 3, 4, 5, \dots$ -times enlarged unit cell [22, 23, 37, 44]. At zero temperature and weak interactions $U/J \rightarrow 0$, the vortex density, as a function of flux ϕ , exhibits the famous devil's staircase structure [44, 45] with a plateau for each commensurate value of ρ_v . The reversal of the current in the VL $_{1/2}$ -SF phase clearly survives a finite temperature, which also applies (though for lower values of temperatures) to the current reversal in the vicinity of the VL $_{1/3}$ -SF state for $\phi < 2\pi/3$. The optimal parameters for observing the current reversal in the weak-coupling regime are $\phi \simeq 0.9\pi$ and $J_{\perp} \simeq 1.2J$ where the reversal is observed for $T < 0.4J/k_B$.

At extremely low temperatures, a reversal of the chiral current for the parameters of Fig. 4 is also visible in the $\rho_v = 2/5$ VL state with $M = 5$ for $\phi \simeq 4\pi/5$ (see the inset in Fig. 4a). Other vortex-lattice states (corresponding to the regions in which plateaux are formed in the $\rho_v = \rho_v(\phi)$ curve in Fig. 4b) do not induce a reversal of the chiral current even at $T = 0$. For instance, consider the vortex lattice with $\rho_v = 1/4$ and $M = 4$: Its region of stability, for the parameters of Fig. 4, corresponds to flux values slightly exceeding $\pi/2$, and thus $\text{sign}[j_c(\phi)] = \text{sign}[j_c(\phi_{\text{eff}})]$, where $\phi_{\text{eff}} = 4\phi$.

A striking feature in the weak-coupling regime is the self-similar structure of the $j_c(\phi)$ curve for $k_B T \ll J$: After the spontaneous M -fold increase of the unit cell, the chiral current exhibits a behavior that is similar to the one in the Meissner phase. For instance, for the VL state at $\rho_v = 1/2$, this is visible in Fig. 4a at a flux value

of $\phi = \pi$ and for VL states at $\rho_v = 1/3$ and $2/5$ in the insets of Fig. 4a at $\phi = 2\pi/3$ and $4\pi/5$, respectively. As a result, the absolute values of the reversed current for $\phi \sim \pi$ are several times larger than in the $U = 0$ case at the same value of ϕ (compare the slopes of the continuous black curve and the red dashed curve in Fig. 4a at $\phi = \pi$).

The transfer-matrix approach further unveils another important result: the VL_{1/2}-SF phase as well as the current reversal associated with it persists down to arbitrarily small values of U at sufficiently low temperatures (see Fig. 4a where in the vicinity of $\phi = \pi$, comparing the $U = 0$ and $0 < U/J \ll 1$ cases, the sign of the chiral current as well as their absolute values differ).

Summary and discussion. We introduced the effect of the spontaneous reversal of the chiral current for interacting bosons in a uniform magnetic field on a two-leg ladder. The effect is the most spectacular and counter-intuitive in the weak-coupling limit, where for values of flux close to $2\pi/3, 4\pi/5$ and π and in the absence of interactions, bosonic particles propagate counterclockwise along the ladder's boundary, whereas for any arbitrarily weak interaction strength and at low temperatures, the direction of the particle flow can get reversed, without changing the external magnetic field. The effect should be readily observable with existing experimental setups with quantum gases in optical lattices [29, 39, 40] and also in Josephson junctions. The current reversal could be used as an indicator of the onset of vortex-lattice phases. The effect described here is not restricted to two-leg ladders. Preliminary results indicate that the chiral-current reversal driven by interactions also exists in the Bose-Hubbard model on three-leg ladders [46].

S.G. and T.V. acknowledge support by QUEST (Center for Quantum Engineering and Space-Time Research) and DFG Research Training Group (Graduiertenkolleg) 1729. We are grateful to E. Jeckelmann, M. Lein and L. Santos for useful discussions. The research of M.P. was supported by the European Union through the Marie-Curie grant ToPOL (No. 624033) (funded within FP7-MC-IEF). I.M.C. acknowledges funding from the Australian Research Council Centre of Excellence for Engineered Quantum Systems and grant number CE110001013.

Methods. (i) *DMRG.* For interaction strengths of $U/J \gtrsim 1$ and particle filling $\rho < 2$, we perform large scale numerical density matrix renormalization group [20, 21] simulations which allow us to calculate zero-temperature properties for open boundary conditions and systems with up to $L = 160$ rungs, using 1000 DMRG states. Since the local Hilbert space of bosons is generally unconstrained we employ a cutoff of the maximal occupation. We typically use a cut-off of four bosons per site which is justified due to the repulsive nature of onsite interactions $U > J$. By comparison with larger and smaller cutoffs we have verified the numerical accuracy of the quantities shown here. Close to the V-SF to VL _{ρ_v} -SF boundaries,

the DMRG simulations tend to converge to metastable excited states with larger or smaller vortex density. Here we have performed several calculations starting from different randomly chosen initial states. Selecting the lowest energy states gives the piecewise continuous chiral-current curve presented in Fig. 3.

(ii) *Transfer-matrix approach for the $\rho \gg 1, U \ll J$ limit.* For large particle densities per ladder site we follow approaches used in the theory of Josephson-junction ladders, where each superconducting island is proximity-coupled to its three neighbors. It is convenient to introduce a density phase representation of bosonic operators $a_{l,r}^\dagger = \sqrt{\rho + \delta\rho_{l,r}} e^{i\theta_{l,r}}$, where $\delta\rho_{l,r} = n_{l,r} - \rho$ and $\theta_{l,r}$ describe the density fluctuations and the phase of the condensate at site (l, r) , respectively. In the limit $U/J \rightarrow 0$, the charging effects of the superconducting islands are negligible (equivalent to neglecting density fluctuations), and the Hamiltonian of equation (1) becomes

$$H \rightarrow -2J\rho \sum_{\ell=1,2;r=1}^L \cos(\theta_{\ell,r+1} - \theta_{\ell,r}) - 2J_\perp \rho \sum_{r=1}^L \cos(\theta_{1,r} - \theta_{2,r} - r\phi). \quad (2)$$

with local variables $\theta_{l,r} \in [0, 2\pi)$. In equation (2), it is more convenient to impose periodic boundary conditions. The transfer matrix \hat{P} , connected with the partition function $Z = \text{tr } \hat{P}^L$ was obtained in [23]. Following [23], we numerically calculated the eigenvalues λ_n of the transfer matrix (where $n = 0, 1, 2, \dots$ and $|\lambda_n| \geq |\lambda_{n+1}|$) in the thermodynamic limit. The periodicity of the argument of the second largest eigenvalue as a function of flux yields the vortex density $\rho_v(\phi) = \text{Arg}[\lambda_1(\phi)]/2\pi$ for different temperatures [23] presented in Fig. 4b. The chiral-current curves corresponding to different temperatures presented in Fig. 4a are obtained from

$$j_c(\phi) = -\frac{k_B T}{N} \frac{\partial \ln Z}{\partial \phi}.$$

SUPPLEMENTARY MATERIAL FOR "SPONTANEOUS INCREASE OF MAGNETIC FLUX AND CHIRAL-CURRENT REVERSAL IN BOSONIC LADDERS: SWIMMING AGAINST THE TIDE"

S1. CHIRAL CURRENT

In the supplementary material we will discuss ground state properties, hence $T = 0$.

The local current operators, defined through the standard lattice version of the continuity equation for particle densities, are denoted by $j_{\ell,r}^\parallel$ (along the links of the ladder legs) and j_r^\perp (on the rungs). Their explicit expressions

are

$$\begin{aligned} j_{\ell,r}^{\parallel} &= iJ \left(a_{\ell,r+1}^{\dagger} a_{\ell,r} - a_{\ell,r}^{\dagger} a_{\ell,r+1} \right) \\ j_r^{\perp} &= iJ_{\perp} \left(e^{-ir\phi} a_{1,r}^{\dagger} a_{2,r} - e^{ir\phi} a_{2,r}^{\dagger} a_{1,r} \right). \end{aligned} \quad (3)$$

In the thermodynamic limit ($L \rightarrow \infty$), where contributions from the rungs at the boundaries ($r = 1$ and $r = L$) of the ladder are negligible, or for periodic boundary conditions, the chiral current becomes

$$j_c = \frac{1}{N} \sum_r \langle j_{1,r}^{\parallel} - j_{2,r}^{\parallel} \rangle = \frac{\partial E_0}{\partial \phi}, \quad (4)$$

where E_0 is the ground-state energy per particle [35].

One can easily show that for non-interacting bosons ($U = 0$) and for $J_{\perp} \leq 2J \sin \frac{\phi}{2} \tan \frac{\phi}{2}$,

$$j_c = \frac{J_{\perp}^2 \sin \phi}{8J \sin^4 \frac{\phi}{2} \sqrt{1 + (J_{\perp}/2J \sin \frac{\phi}{2})^2}}. \quad (5)$$

For $U = 0$, the chiral current saturates at $j_c = J \sin \frac{\phi}{2}$ in the Meissner-superfluid phase, i.e., for $J_{\perp} > 2J \sin \frac{\phi}{2} \tan \frac{\phi}{2}$.

In the complementary regime of strongly interacting bosons $U \gg J$, we also observe a quadratic dependence of j_c on J_{\perp} for small values of J_{\perp}/J . In fact, such a dependence holds for arbitrary values of U/J for $J_{\perp} \ll J\phi$ [35]. For strong hopping on the rungs $J_{\perp} \gg J$ and for very strong interactions $U/J \rightarrow \infty$, the chiral current can decay to zero in the Mott-insulating states even at half-integer filling. For instance, for $\rho = 0.5$, the chiral current is $j_c = J^2 \sin \phi / (2J_{\perp})$ [35]. Both in the $U = 0$ and the $U/J \rightarrow \infty$ regime, the particles circulate counterclockwise along the boundary given that $0 < \phi < \pi$.

S2. FINITE-SIZE DEPENDENCE OF THE CHIRAL CURRENT

In Fig. 3 of the main text, we presented results for the chiral current for the largest system size ($L = 160$) used in our DMRG simulations. Strong finite-size effects are present in the vortex-liquid phase (V-SF). In Fig. 5, we further illustrate these finite-size effects by showing additional results for the chiral current for systems with $L = 80, 120$ and 160 rungs. By contrast, in the vortex-lattice phases finite-size effects are practically invisible on the scale of the figure.

As one can see in Fig. 5, upon increasing system size, the width of the small quasi-plateaux of almost constant chiral current present in the V-SF phases diminishes, indicating that in the thermodynamic limit, the chiral current will become a continuous function of the flux in all phases as well as at the phase transitions between the vortex-liquid and the vortex-lattice phases presented in

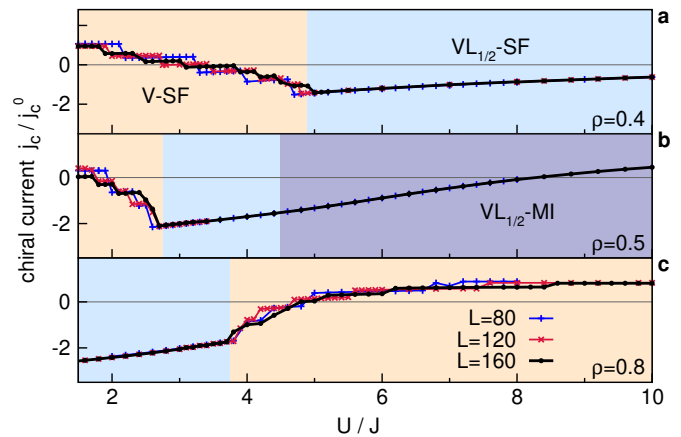


FIG. 5. *Finite-size dependence of the chiral current.* We plot j_c as a function of interaction strength U/J for the parameters of Fig. 3 of the main text ($\phi = 0.9\pi$, $J_{\perp} = 1.6J$). The figure shows results for three system sizes [$L = 80$ (blue symbols), $L = 120$ (red symbols) and $L = 160$ (black symbols)] and for particle densities $\rho = 0.4$ (a) (not shown in the main text), $\rho = 0.5$ (b) and $\rho = 0.8$ (c). Due to the incommensurate vortex density a significant system-size dependence is present in vortex-liquid superfluid states (V-SF), as opposed to the behavior in vortex-lattice states.

Fig. 3 of the main text. For a filling of $\rho = 1$ (presented in Fig. 3c of the main text), the transition from the vortex lattice into a vortex-liquid state happens inside the Mott-insulating phase, with finite-size effects being much less severe (not shown here).

S3. GROUND-STATE PHASES

We next present the phase diagram of the model in the (ϕ, J_{\perp}) plane for a moderate strength of the interaction of $U/J = 2$ and a non-integer filling in Fig. 6a. It is quite remarkable that this ground-state phase diagram is so rich, with a plethora of superfluid phases. Besides the Meissner superfluid (M-SF), the vortex liquid (V-SF), and the $VL_{1/2}$ -SF, a $VL_{1/3}$ -SF can get stabilized with a spontaneously tripled unit cell. However, the stability domain of the $VL_{1/3}$ -SF (for the parameters of Fig. 6a) corresponds to flux values $\phi > 2\pi/3$ and therefore, the increased (tripled) effective flux in the $VL_{1/3}$ -SF state does not result in a current reversal, confirmed by our simulations. For larger values of J_{\perp}/J , an additional phase, predicted in mean-field approximation [33], with a spontaneously emerging imbalance in the particle numbers on the two legs exists, dubbed biased leg phase (BLP). This phase, however, preserves the original unit cell and thus does not trigger a chiral-current reversal either (see Fig. 9).

In Fig. 6b, we present the phase diagram as a function

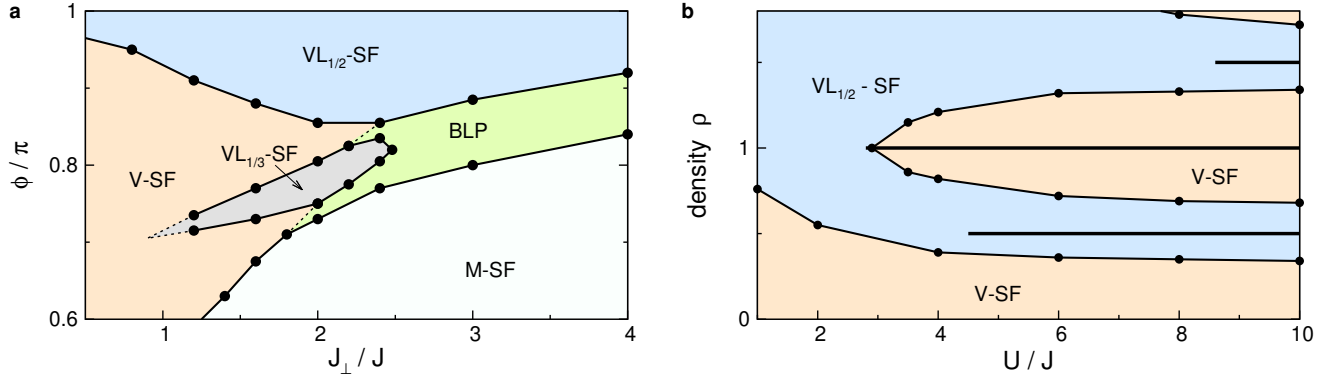


FIG. 6. *Ground-state phase diagram.* **a**, Phase diagram in the parameter plane (ϕ, J_{\perp}) for $\rho = 0.8$ and $U = 2J$. **b**, Phase diagram in the (ρ, U) plane for $\phi = 0.9\pi$ and $J_{\perp} = 1.6J$. The horizontal bold lines indicate Mott-insulating phases at commensurate fillings of $\rho = 0.5, 1, 1.5$. Apart from the Meissner (M-SF, white), vortex-liquid (V-SF, orange) and vortex-lattice superfluids (VL $_{1/2}$ -SF, blue, and VL $_{1/3}$ -SF, gray) phases, another superfluid phase with a particle number imbalance between the two legs emerges, the biased leg phase (BLP, green) [33].

of ρ and U/J for $\phi = 0.9\pi$, $J_{\perp} = 1.6J$, $\rho < 2$ and $U \geq J$. The vortex lattice with $\rho_v = 1/2$ exists in a wide parameter range at sufficiently large densities (the critical lower density is U -dependent) and, for larger $U/J \gtrsim 4$, is interlaced multiple times by the V-SF phase as density increases. Moreover, there are Mott-insulating phases at densities $\rho = 1/2, 1, 3/2$ [32, 35, 47]. The transition from the VL $_{1/2}$ -SF into the V-SF phase induced by changing U or ρ is caused by a proliferation of soliton-anti-soliton pairs in the V-SF state (see Fig. 7b1).

The superfluid vortex liquid (V-SF) is the only two-component Luttinger liquid [35] (central charge $c = 2$), while all other superfluid phases are one-component Luttinger liquids ($c = 1$). The vortex-lattice and Meissner phases are identified by their characteristic local current configurations as shown in the following section. They may be clearly discriminated from the vortex-liquid phase by calculating the central charge c extracted from entanglement-scaling properties [48, 49] (results not shown here, see [35] for examples).

All phase transitions in Figs. 6a and b are second-order commensurate-incommensurate transitions [37], except for those into the BLP phase, which are identified by sharply increasing particle density imbalance between the legs $\Delta n = \sum_r (n_{1,r} - n_{2,r})/N$.

There are also isolated Berezinskii-Kosterlitz-Thouless (BKT) [50, 51] critical points from Mott-insulating (vortex lattice) phases to superfluid (vortex-liquid) states, along the paths of a constant particle (vortex) density. The BKT transitions between VL $_{1/2}$ -SF and VL $_{1/2}$ -MI at fillings $\rho = 0.5$ and $\rho = 1.5$ shown in Fig. 6b are determined by numerically analyzing correlation functions. At the transition from the VL $_{1/2}$ -SF to the VL $_{1/2}$ -MI, bosonization predicts that the single-particle correlation function decay as $\langle a_{l,r}^{\dagger} a_{l,r+x} \rangle \sim x^{-\frac{1}{4}}$ (up to logarithmic corrections). The transition point can be extracted ac-

curately from the finite-size scaling behavior of peaks in the quasi-momentum distribution function [52].

For the BKT transition from the superfluid to the Mott insulator at unit filling $\rho = 1$, which happens inside the vortex lattice at $\rho_v = 1/2$ state presented in Fig. 6b, it can be shown using bosonization that the single-particle correlation function decays as $\langle a_{l,r}^{\dagger} a_{l,r+x} \rangle \sim x^{-\frac{1}{8}}$ (up to logarithmic corrections). The VL $_{1/2}$ -MI to V-MI phase transition point is located from the behavior of the chiral current as well as from the local-current structure while the transition from the V-MI to the M-MI is determined by analyzing local current structure (these transitions are not indicated in the figure).

S4. LOCAL CURRENTS, PARTICLE DENSITIES AND CHIRAL CURRENT IN DIFFERENT PHASES

The different superfluid phases discussed in the main text can be distinguished from each other by the structure of local particle currents and local particle densities. In Fig. 7, we present typical examples for a cut through the phase diagram Fig. 6a at $J_{\perp} = 1.6J$. We show results for a central portion of the ladder with $L = 120$ rungs.

Upon increasing ϕ (from bottom to top in Fig. 7), the system passes from the Meissner phase [M-SF, Figs. 7e1-e3] (stable for $\phi \lesssim 0.7\pi$) to the vortex-lattice state VL $_{1/2}$ -SF (shown in Figs. 7a1-a3, realized for $\phi \sim \pi$) by going through additional intermediate vortex-liquid and vortex-lattice phases. As already mentioned, in the Meissner phase, currents are non-zero only along the ladder's legs (and, for open boundary conditions, also on the boundary rungs $r = 1$ and $r = L$, not shown), hence the vortex density ρ_v vanishes, while the particle density is uniform in the bulk of the ladder. Adjacent to the Meissner phase, there is a vortex-liquid superfluid (V-SF) with

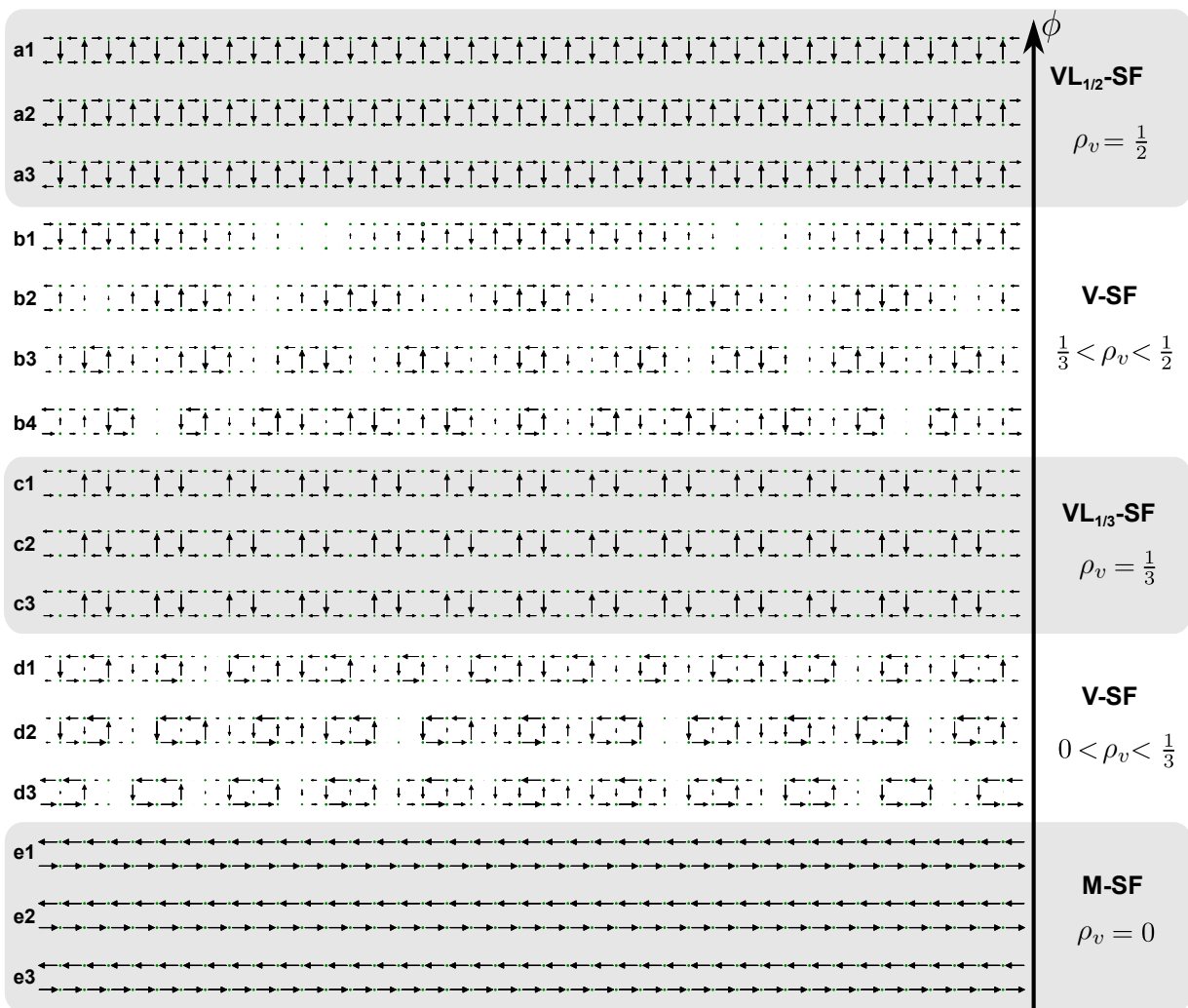


FIG. 7. *Configurations of local currents and densities in various phases.* DMRG results are presented along the cut at $J_{\perp} = 1.6J$ through the phase diagram Fig. 6a for $0.5\pi < \phi < \pi$. The parameters of Fig. 6a are $U = 2J$ and $\rho = 0.8$. The configurations presented here correspond to the following flux values in descending order: 0.95π (**a1**), 0.93π (**a2**), 0.9π (**a3**), 0.88π (**b1**), 0.86π (**b2**), 0.82π (**b3**), 0.79π (**b4**), 0.77π (**c1**), 0.75π (**c2**), 0.73π (**c3**), 0.71π (**d1**), 0.69π (**d2**), 0.68π (**d3**), 0.64π (**e1**), 0.6π (**e2**) and 0.56π (**e3**) (DMRG data for $L = 120$ rungs). We only depict the behavior for the middle rungs of the ladder ($40 \leq r \leq 80$) in the bulk of the system. The local currents and local particle densities presented in Fig. 2c of the main text in the $VL_{1/3}$ -SF and $VL_{1/2}$ -SF are cut from the central region of configurations **c2** and **a3** presented here. The length of the arrows encodes the absolute value of the local currents and the size of the circles encodes the on-site density. In the top four configurations **a1**- **b1**, the chiral current is reversed and circulates in clockwise direction.

a finite vortex density $0 < \rho_v < 1/3$ (shown in Figs. 7d1-d3). For values of $0.75\pi \lesssim \phi \lesssim 0.82\pi$, the vortex-lattice phase with $\rho_v = 1/3$ ($VL_{1/3}$ -SF) becomes the ground state (shown in Figs. 7c1-c3). Both local currents along the legs and along the rungs have a periodicity with a period of three times the lattice spacing, which is also exhibited by the local particle density.

Upon further increasing the flux but still before the vortex lattice at $\rho_v = 1/2$ ($VL_{1/2}$ -SF) is stabilized, the system reenters the vortex-liquid phase with vortex densities $1/3 < \rho_v < 1/2$ (shown in Figs. 7b1-b4). In the vortex-liquid state and in the proximity of the $VL_{1/2}$ -SF, domain walls (or solitons) between the two degenerate

ground states of the $VL_{1/2}$ -SF state, which we denote by $|1\rangle$ and $|2\rangle$, are clearly visible (see Fig. 7b1 and b2). We call a soliton a defect in the periodic structure of the $VL_{1/2}$ -SF state with a $|1\rangle$ -like pattern to the left of the defect and a $|2\rangle$ -like pattern to the right side and anti-solitons a defect with a $|2\rangle$ -type pattern on the left side and a $|1\rangle$ -type pattern on the right side. The number of solitons and anti-solitons in the vortex-liquid state in the vicinity of $VL_{1/2}$ -SF are identical, due to the topological confinement stemming from the double degeneracy of the ground state of the $VL_{1/2}$ -SF phase. The local density shows modulations near the positions of solitons and anti-solitons. In the $VL_{1/2}$ -SF state, on the contrary, the

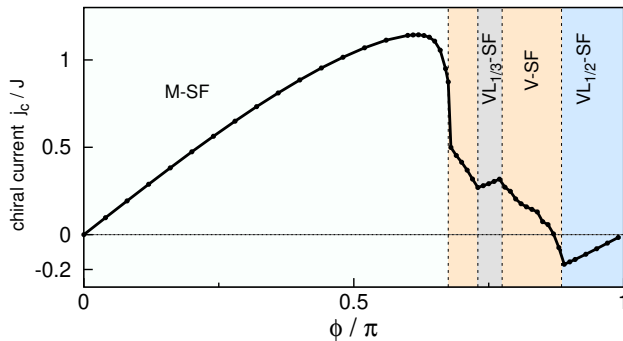


FIG. 8. *Flux dependence of the chiral current.* We display DMRG results for the chiral current along the cut at $J_{\perp} = 1.6J$ through Fig. 6a ($U = 2J$ and $\rho = 0.8$) for $0 < \phi \leq \pi$, obtained for $L = 120$ rungs.

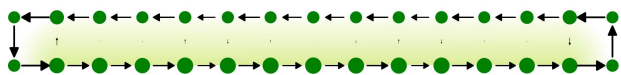


FIG. 9. *Typical pattern of local currents and local densities in the biased leg phase (BLP).* In the particular realization shown here the lower leg hosts the majority of particles. These DMRG results are for the parameters of Fig. 6a ($\rho = 0.8$ and $U = 2J$) and for a point inside the BLP phase ($\phi = 0.8\pi$, $J_{\perp} = 2.7J$, $L = 15$). The length of the arrows encodes the strength of local currents and the size of the circles is proportional to the density.

local densities are constant in the bulk along the ladder and the local currents show a modulation with a period of two lattice cells. In general, in vortex-liquid phases, the particle density and local currents exhibit a complicated structure, unlike the highly regular patterns of the vortex-lattice states.

While additional vortex-lattice phases with a vortex density higher than $\rho_v = 1/2$ (specifically, $\rho_v = 2/3$ and $\rho_v = 1$) have been suggested [37], the maximal possible vortex density in this system can in fact not exceed $\rho_v = 1/2$. This limit is reached for values of the flux $\phi \sim \pi$ for any choice of parameters, in agreement with the picture originating from the weak-coupling regime $\rho \gg 1$, $U/J \rightarrow 0$ [23, 44]. The current configurations presented in our $VL_{1/3}$ -SF phase, here obtained from our numerical simulations and shown in Figs. 7c1-c3 are different from those depicted in [32, 37]. Namely, and most importantly around the vortices, particles circulate in the direction opposite to the behavior in the Meissner phase. Hence, the vortices that we observe resemble the vortices of type-II superconductors. We further note that in $VL_{1/3}$ -SF vortex lattices, the particle density is reduced at the corners of those plaquettes at which the vortices sit, which is not captured in the standard linearized bosonization approach used in [32, 34, 35, 37]. By contrast, in the $VL_{1/2}$ -SF, vortices occupy every other

plaquette and hence there is no corresponding effect on the local particle density. The density pattern of the $VL_{1/3}$ -SF state is, however, inhomogeneous, yet nevertheless follows the periodicity of the local current configuration of the underlying vortex-lattice state: Vortices sit in regions of lower particle density. In the $VL_{1/3}$ -SF, a periodically modulated local current and a periodic density modulation coexists with superfluidity.

Unlike linearized bosonization, a mean-field approach [33] yields a modulation of the particle density in vortex phases. However, in mean-field theory and at $\phi = \pi$, the particle density is modulated from rung to rung with a period of two lattice constants, whereas our numerical simulations for fluxes close to π (including $\phi = \pi$) produce $VL_{1/2}$ -SF states with a uniform particle density along the ladder.

The dependence of the chiral current as a function of flux ϕ and as the system goes through the different ground-state configurations shown in Fig. 7 is presented in Fig. 8. For $J_{\perp} = 1.6J$, the chiral current does not undergo a sign reversal in the $VL_{1/3}$ -SF state, since this state is stabilized only for $\phi > 2\pi/3$. A reversal occurs only near $\phi \sim \pi$. Note that even though generically, the transition from Meissner to vortex-liquid phases is a second-order commensurate-incommensurate transition, in the numerical data for finite system sizes shown in Fig. 8, there is a finite jump in the chiral current. We attribute this to the proximity of the multicritical point at which the Meissner superfluid phase, the vortex superfluid and the BLP phases meet (see Fig. 6a).

For completeness we also present results for the typical behavior of local currents and particle densities in the BLP phase, obtained from DMRG simulations for $L = 15$, shown in Fig. 9 (we choose a small system to illustrate the behavior on the boundary rungs $r = 1$ and $r = L$ as well). The local currents are non-zero along the legs and edge rungs of the ladder and particles flow in counter-clockwise direction. The absolute values of local currents (which for a finite system depend on the distance from the edge rungs) are identical in both legs, while the density is imbalanced between the two legs. Thus, one can deduce that the behavior of the chiral current in the BLP superfluid is quite similar to that in the Meissner superfluid, where particles circulate along the ladder's boundary, vanishing quickly on the rungs in the bulk since $\rho_v = 0$). Nevertheless, the BLP phase is distinct from the M-SF since in the former there is a spontaneously broken discrete Z_2 symmetry corresponding to time reversal combined with exchange of the legs.

-
- [1] L. De Broglie, University of Paris (1924).
 - [2] S. Bose, *Zeitschrift für Physik* **26**, 178 (1924).
 - [3] A. Einstein, *Sitzungsberichte der Preussischen Akademie*

- der Wissenschaften **1**, 3 (1925).
- [4] M. Anderson, J. Ensher, M. Matthews, C. Wieman, and E. Cornell, *Science* **269**, 198 (1995).
- [5] K. B. Davis, M. O. Mewes, M. R. Andrews, N. J. van Druten, D. S. Durfee, D. M. Kurn, and W. Ketterle, *Phys. Rev. Lett.* **75**, 3969 (1995).
- [6] P. Kapitza, *Nature* **141**, 74 (1938).
- [7] J. F. Allen and A. D. Miesener, *Nature* **141**, 75 (1938).
- [8] L. D. Landau, *J. Phys. (USSR)* **5**, 71 (1941).
- [9] N. N. Bogoliubov, *J. Phys. (USSR)* **11**, 23 (1947).
- [10] L. Onsager, *Nuovo Cimento* **6 Supp. 2**, 279 (1949).
- [11] R. P. Feynman, *Progress in Low Temperature Physics* **1**, 36 (1955).
- [12] W. Vinen, *Nature* **181**, 1524 (1958).
- [13] P. Engels, I. Coddington, P. C. Haljan, and E. A. Cornell, *Phys. Rev. Lett.* **89**, 100403 (2002).
- [14] M. W. Zwierlein, J. R. Abo-Shaeer, A. Schirotzek, C. H. Schunck, and W. Ketterle, *Nature (London)* **435**, 1047 (2005).
- [15] N. R. Cooper, *Advances in Physics* **57**, 539 (2008).
- [16] A. A. Abrikosov, *JETP* **5**, 1174 (1957).
- [17] D. Cribier, B. Jacrot, L. Madhav, and B. Farnoux, *Phys. Lett.* **9**, 106 (1964).
- [18] U. Essmann and H. Träuble, *Phys. Lett. A* **24**, 526 (1967).
- [19] D. Hügel and B. Paredes, *Phys. Rev. A* **89**, 023619 (2014).
- [20] S. R. White, *Phys. Rev. Lett.* **69**, 2863 (1992).
- [21] U. Schollwöck, *Rev. Mod. Phys.* **77**, 259 (2005).
- [22] M. Kardar, *Phys. Rev. B* **33**, 3125 (1986).
- [23] C. Denniston and C. Tang, *Phys. Rev. Lett.* **75**, 3930 (1995).
- [24] A. van Oudenaarden and J. E. Mooij, *Phys. Rev. Lett.* **76**, 4947 (1996).
- [25] A. van Oudenaarden, S. J. K. Várdu, and J. E. Mooij, *Phys. Rev. Lett.* **77**, 4257 (1996).
- [26] D. Rodichev, C. Brun, L. Serrier-Garcia, J. C. Cuevas, V. H. L. Bessa, M. V. Milosevic, F. Debotridder, V. Stolyarov, and T. Cren, *Nature Phys.* **11**, 332 (2015).
- [27] M. Greiner, O. Mandel, T. Esslinger, T. Hänsch, and I. Bloch, *Nature (London)* **415**, 39 (2002).
- [28] I. Bloch, J. Dalibard, and W. Zwerger, *Rev. Mod. Phys.* **80**, 885 (2008).
- [29] M. Atala, M. Aidelsburger, M. Lohse, J. T. Barreiro, B. Paredes, and I. Bloch, *Nature Phys.* **10**, 588 (2014).
- [30] H. Miyake, G. A. Siviloglou, C. J. Kennedy, W. C. Burton, and W. Ketterle, *Phys. Rev. Lett.* **111**, 185302 (2013).
- [31] M. Aidelsburger, M. Atala, M. Lohse, J. T. Barreiro, B. Paredes, and I. Bloch, *Phys. Rev. Lett.* **111**, 185301 (2013).
- [32] A. Petrescu and K. Le Hur, *Phys. Rev. Lett.* **111**, 150601 (2013).
- [33] R. Wei and E. J. Mueller, *Phys. Rev. A* **89**, 063617 (2014).
- [34] A. Tokuno and A. Georges, *New J. Phys.* **16**, 073005 (2014).
- [35] M. Piraud, F. Heidrich-Meisner, I. P. McCulloch, S. Greschner, T. Vekua, and U. Schollwöck, *Phys. Rev. B* **91**, 140406(R) (2015).
- [36] A. Petrescu and K. Le Hur, *Phys. Rev. B* **91**, 054520 (2015).
- [37] E. Orignac and T. Giamarchi, *Phys. Rev. B* **64**, 144515 (2001).
- [38] W. Meissner and R. Ochsenfeld, *Naturwissenschaften* **21**, 787 (1933).
- [39] B. K. Stuhl, H.-I. Lu, L. M. Ayccock, D. Genkina, and I. B. Spielman, , arXiv:1502.02496 (unpublished).
- [40] M. Mancini, G. Pagano, G. Cappellini, L. Livi, M. Rider, J. Catani, C. Sias, P. Zoller, M. Inguscio, M. Dalmonte, and L. Fallani, , arXiv:1502.02495 (unpublished).
- [41] A. Celi, P. Massignan, J. Ruseckas, N. Goldman, I. Spielman, G. Juzelinis, and M. Lewenstein, *Phys. Rev. Lett.* **112**, 043001 (2014).
- [42] A. Dhar, M. Maji, T. Mishra, R. V. Pai, S. Mukerjee, and A. Paramekanti, *Phys. Rev. A* **85**, 041602 (2012).
- [43] A. Dhar, T. Mishra, M. Maji, R. V. Pai, S. Mukerjee, and A. Paramekanti, *Phys. Rev. B* **87**, 174501 (2013).
- [44] J. J. Mazo, F. Falo, and L. M. Floria, *Phys. Rev. B* **52**, 10433 (1995).
- [45] S. Aubry, *Lect. Notes Math.* **925**, 221 (1982).
- [46] F. Kolley, M. Piraud, I. McCulloch, U. Schollwöck, and F. Heidrich-Meisner, , in preparation (2015).
- [47] F. Crépin, N. Laflorencie, G. Roux, and P. Simon, *Phys. Rev. B* **84**, 054517 (2011).
- [48] P. Calabrese and J. J. Cardy, *J. Stat. Mech.: Theory Exp.* , P06002 (2004).
- [49] G. Vidal, J. I. Latorre, E. Rico, and A. Kitaev, *Phys. Rev. Lett.* **90**, 227902 (2003).
- [50] V. L. Berezinskii, *Sov. Phys. JETP* **34**, 610 (1972).
- [51] J. M. Kosterlitz and D. J. Thouless, *J. Phys. C* **6**, 1181 (1973).
- [52] S. Greschner, L. Santos, and T. Vekua, *Physical Review A* **87**, 033609 (2013).